Inhibition of corrosion driven delamination on iron by smart-release bentonite cation-exchange pigments studied using a scanning Kelvin probe technique

G. Williams*, H.N. McMurray
Materials Research Centre
College of Engineering
Swansea University, Bay Campus
Crymlyn Burrows, Fabian Way
Swansea, SA1 8EN, U.K.
*Corresponding author, email: Geraint.williams@swansea.ac.uk

Abstract: Low-cost, environmentally friendly, cation exchange pigments derived from naturally occurring bentonite clay are shown to significantly enhance resistance to corrosion-driven cathodic delamination in organic coatings adherent to iron surfaces. A scanning Kelvin probe (SKP) is used to study the delamination kinetics of pigmented and unpigmented poly-vinyl-butyral (PVB)-based coatings adherent to polished iron substrates. The bentonite clay is used both in its native form and exhaustively exchanged with a range of divalent alkali earth and trivalent rare earth metal cations. For the best performing divalent cation-exchanged pigment, the dependence of coating delamination rate on pigment volume fraction is determined and compared with that of a conventional strontium chromate ($SrCrO_4$) inhibitor. An inhibition mechanism is proposed for the bentonite pigments whereby underfilm cation release and subsequent precipitation of sparingly soluble hydroxides reduces the conductivity of the underfilm electrolyte.

1. Introduction

The corrosion-driven cathodic delamination of organic coatings adherent to iron and zinc substrates has been shown to proceed via the establishment of an underfilm corrosion cell. Anodic metal dissolution at a penetrative coating defect is coupled to cathodic oxygen reduction occurring near site of coating disbondment by a thin layer of electrolyte ingressing beneath the delaminated coating. [1,2,3,4,5,6,7,8,9,10,11,12] The alkaline environment which forms at the cathode promotes coating disbondment through dissolution of amphoteric oxide layers, polymer degradation, and hydrolysis of interfacial bonds. [2,3,5,7,9] Delamination rates may be reduced by incorporation into the organic coating of corrosion inhibitor pigments, of which strontium chromate ($SrCrO_4$) is the most widely used. However, the known toxicity and carcinogenicity of chromates have resulted in increasing pressure to develop practical alternatives. One of the most promising alternative technologies presently under investigation is the application of ion-exchange materials as so-called "smart-release" pigments incorporated within an organic polymer binder. These systems are "smart" because they release inhibitor species and sequester aggressive ions (e.g. chloride or H^+ ions) only when a corrosive aqueous environment is encountered. A second advantage is that they can be used as generic inhibitor delivery system, within which it is theoretically possible to incorporate any ionic species which can act as a corrosion inhibitor. Therefore, using this type of technology, the range of inhibitors which can be included within a coating is no longer constrained to ionic combinations which form sparingly soluble salts.

In this work we report the use of bentonite cation exchange clays as smart release pigments and describe a program of research to assess their anti-corrosion efficiency when dispersed in a model organic coating applied to iron substrates. Bentonite clays are a form of montemorillonite and exhibit intrinsic cation exchange properties, which are substantially independent of pH. [13,14,15] We have prepared a range of bentonite based pigments containing divalent alkaline-earth and trivalent rare-earth metal cations, specifically designed to inhibit the under-film cathodic disbondment process. Such pigments have previously shown promise in fully formulated organic coating applied to galvanised steel surfaces. [16] A similar approach to the one adopted herein has been used successfully in previous work on galvanised steel to identify promising in-coating cationic inhibitors of underfilm corrosion occurring by a cathodic delamination mechanism [17, 18]. Cations of this type are relatively non-toxic and are known to inhibit corrosion through the deposition of films capable of stifling cathodic

oxygen reduction. [19,20,21,22,23,24]. In the case of galvanised steel, previous work showed that in-coating Zn^{2+} acted considerably more effectively than either group II or rare earth metal cations as inhibitors of cathodic disbondment. [18] The improved efficiency in this case was attributed to the additional ability of interfacial Zn^{2+} to stabilise the amphoteric zinc oxide layer in the event of underfilm alkalisation caused by cathodic oxygen reduction.

The investigation of electrochemical processes within the delamination cell has been facilitated by development of the scanning Kelvin probe (SKP) technique, which allows the spatial and temporal resolution of potential distributions beneath organic coatings. [8,10,11,12] In the work described here, the SKP has been used to follow the delamination kinetics of model coatings from pure iron surfaces. These coatings comprise films of polyvinyl-butyral (PVB) in which have been dispersed varying concentrations of alkaline earth and rare earth cation-exchanged bentonite. Aerated aqueous sodium chloride (NaCl) has been used as the experimental electrolyte in order to reflect standard accelerated corrosion test conditions. The principal aim has been to evaluate the various cation-exchanged bentonites as inhibitors of corrosion-driven cathodic delamination on iron. In so doing, we have also sought to clarify the mechanism by which underfilm cation-exchange leads to the inhibition of cathodic disbondment. In addition, we have also investigated the performance of a benchmark strontium chromate anti-corrosion pigment under identical conditions so that a judgement can be made of the potential viability of smart–release bentonite pigments as Cr (VI) replacement materials.

2. Experimental Details

2.1 Materials

Polyvinyl butyral-co-vinyl alcohol-co-vinyl acetate (PVB), MW *ca.* 100,000, was obtained from the Aldrich Chemical Co. Iron sheet of 1mm thickness and >99.9% purity was obtained from Goodfellow Metals. A commercial grade strontium chromate pigment (primary particle size 1-3 μm) was obtained as dispersion in xylene from Akzo Nobel Industrial Coatings. Wyoming Bentonite (grade GG, cation exchange capacity 0.7 milli-equivalents per gram) was obtained from Steetley Bentonites and Absorbents. Bentonite samples were exhaustively exchanged with divalent alkaline earth (Ca^{2+}, Mg^{2+}, Sr^{2+}, Ba^{2+}) or trivalent rare earth (Ce^{3+},

Y^{3+}) cations from aqueous solutions of alkaline earth chloride or rare earth chlorides (99.9% purity, Aldrich) using a literature method. [25] The resulting cation exchanged bentonites were then washed by repeated cycles of centrifugation and re-dispersion in fresh distilled water until Cl^- ions could no longer be detected in the washing liquor using silver nitrate solution. Finally, the bentonites were washed with ethanol, dried in an oven at 70°C for four hours, and the resulting powder ground to give a particle size of < 20 μm diameter. Chemical analysis of selected bentonite pigments was carried out by digestion in aqua regia followed by inductively coupled plasma / mass spectrometry. The Ca^{2+} and Ce^{3+} exchanged bentonite pigments were found to contain 1.35% w/w calcium and 3.15% w/w cerium respectively. Dispersions of the Ca^{2+} and Ce^{3+} bentonites in water (5% w/w) both exhibited a pH of *ca.* 6.5.

2.2 Methods

The design and operation of the SKP apparatus used here has been described in detail elsewhere, [12, 26] as has the procedure for calibrating the SKP in terms of local free corrosion potential (E_{corr}). [12] Following this calibration procedure it was shown that for a metal surface covered with an adherent PVB film or with a PVB film which has become delaminated through the ingress of a thin electrolyte film,

$$E_{\mathrm{corr}} = \Delta\psi_{\mathrm{Pol}}^{\mathrm{Ref}} + 0.33\ \mathrm{V}\ \textit{vs.}\ \mathrm{SHE} \qquad (1)$$

where $\Delta\psi_{\mathrm{Pol}}^{\mathrm{Ref}}$ is the Volta potential difference measured between the SKP reference probe and the polymer-air interface.

Iron samples for delamination experiments were polished using an aqueous slurry of 5 μm Alumina powder, followed by cleaning in a non-ionic surfactant, rinsing, degreasing with acetone and air drying. PVB solutions (15.5% w/w) were prepared in ethanol, with any required amount of pigment added as a dispersion in the minimum volume of ethanol, followed by thorough mixing using a high shear blender. PVB coatings were applied to the iron substrate and air-dried to give a strongly adherent film of 30 μm thickness, as determined using a micrometer screw gauge. [12] Following the approach of Stratmann et al.,[10] a coating defect was then created by cutting and lifting the clear adhesive tape to reveal a 20 ×15 mm area of bare metal to which electrolyte was subsequently applied.

All delamination experiments were carried out at 25°C using 0.86 M aqueous NaCl at pH 6.5. The sample was mounted in the closed environment chamber of the SKP apparatus and allowed to equilibrate with an atmosphere maintained at *ca.* 95% relative humidity by a reservoir of experimental electrolyte for a period of six hours. An aliquot of electrolyte was then applied to the artificial defect to create a 1 mm thick electrolyte layer and initiate delamination. The SKP reference probe was scanned over the coated surface along a 12 mm line normal to, and adjacent with the defect-coating boundary. Scans were conducted immediately after the addition of electrolyte and thereafter at hourly intervals over a 24h period using a reference probe-to-sample air gap of 100 μm and recording 20 E_{corr} data points per mm.

Samples used to investigate the susceptibility of pigmented-PVB coated iron substrates to underfilm corrosion via an anodic disbondment (filiform corrosion) mechanism were prepared in a slightly different way. [27], The iron surface was coated with an ethanolic solution of PVB as described above, but the coating defect was created by a scribing a central region of the coated surface (2 mm) using a scalpel blade. Underfilm corrosion was initiated by applying a 2 μL quantity of 0.01 mol dm^{-3} NaCl (aq) to the coating defect by means of a microlitre syringe. The sample was subsequently maintained in air at 20°C and 95% relative humidity for periods of up to several days and subjected to continuous in situ SKP scanning of a 1 cm^2 area centred on the penetrative coating defect. Secondary ion mass-spectroscopy (SIMS) was used to analyse post-corrosion iron substrate surfaces. After a period of 24 h maintained in a closed chamber at a constant relative humidity of 96%, the coating was carefully peeled away. SIMS analysis was carried out on the underlying Fe surface using a Millbrook Instruments MC300 (Mk II) mini-SIMS fitted with a Gallium ion source having a lateral resolution of 10 μm and a mass resolution of ± 0.1 Dalton.

3. Results

3.1 Inhibition of coating failure by a cathodic disbondment mechanism

Delamination experiments were carried out using unpigmented PVB coatings in order to establish baseline delamination kinetics. Following equilibration with the humid experimental atmosphere, E_{corr} values over the intact coating surface, as obtained from experimental $\Delta\psi_{Pol}^{Ref}$ values using equation (1) were uniformly high and similar to the uncoated iron surface under the same conditions, ie. ca. +0.1 – +0.2 V vs. SHE. Upon addition of 0.86 mol dm^{-3} NaCl (aq) to the defect area the bare metal surface became visibly corroded within minutes. Coating delamination typically became initiated within 1 hour of electrolyte contact. As delamination proceeded, distinctive time-dependent E_{corr} - distance profiles became established as shown in Figure 1. It may be seen from Fig. 1 that a sharp potential drop of ca. 0.2 V occurs in the immediate vicinity of the delamination front. A more gradual, approximately linear, drop in potential then links the delamination front to the region adjacent to the coating defect, where potentials ultimately fall to between –0.4 and –0.5 V. Only very limited tarnishing of the iron surface was observable beneath the delaminated coating.

Preliminary delamination experiments intended to establish the relative inhibition efficiency of group II and rare-earth (RE) cation-exchanged bentonite pigments were carried out using PVB coatings containing a fixed pigment volume fraction (ϕ) of 0.1. Regardless of the type of pigment used, E_{corr} values over the intact coating surface remained similar to that for unpigmented PVB. Consequently, there is no reason to suggest that either group II or RE cation-exchanged bentonites significantly influence polarisation of the intact iron-coating interface. Figure 2 shows typical E_{corr} versus distance profiles measured in the presence of dispersed Y^{3+}-exchanged bentonite (Ben-Y^{3+}) pigment at ϕ = 0.l. Entirely similar E_{corr} versus distance profiles were also obtained when Mg^{2+}, Ca^{2+} , Sr^{2+}, Ba^{2+} and Ce^{3+}-exchanged bentonites were incorporated within the PVB coating using at the same ϕ value. Upon the establishment of a delamination cell, Figure 2 shows that E_{corr} values measured in the vicinity of the defect edge are similar to those expected for the equilibrium potential of the Fe/Fe^{2+} redox couple. Accordingly, there is no reason to propose that group II and RE cations released through ion exchange significantly influence polarisation (anodic or cathodic) of the Fe–electrolyte interface at the coating defect. The inset in Fig 2 shows plots of the time-dependent distance (from the defect edge) over which delamination has occurred (x_{del}), plotted as a function of $(t_{del} - t_i)^{1/2}$, which compare the delamination kinetics obtained from the Ben-Y^{3+} inhibited coating with unpigmented PVB. From this, it can be seen that the delamination kinetics remain parabolic in the presence of the pigment, where t_{del} is the electrolyte contact

time and t_i is for the time taken for the delamination cell to become established. Again, entirely similar results were obtained using Mg^{2+}, Ca^{2+} , Sr^{2+}, Ba^{2+} and Ce^{3+}-exchanged bentonite pigments, although the slopes of the x_{del} vs. $(t_{del} - t_i)^{1/2}$ plots (k_{del}) varied between a minimum of 0.012 to a maximum value of 0.079 mm $min^{-1/2}$, determined for Ben-Ca^{2+}- and Ben-Ce^{3+} pigments respectively. The various parabolic delamination rate constant (k_{del}) values obtained from preliminary screening experiments at $\phi = 0.1$ are compared in the bar chart given in Figure 3. It is evident that the unexchanged bentonite, containing native Na^+ exchangeable cations, accelerated the rate of coating delamination, compared with the unpigmented PVB coating, while all other bentonite pigments produced a profound decrease in k_{del}. It can also be seen that the best performing bentonite pigment, Ben-Ca^{2+}, produced a very similar delamination rate to a benchmark $SrCrO_4$ pigment at the same volume fraction.

The effect of varying ϕ on coating disbondment rates was subsequently systematically investigated for the best performing bentonite system (Ben-Ca^{2+}) only. Experiments were carried out using a series of PVB-coated iron samples incorporating dispersions of Ben-Ca^{2+} pigment at levels of $0.01 \leq \phi \leq 0.2$. Figures 4a and 4b show E_{corr} versus distance profiles for determined for PVB coatings containing dispersed Ca^{2+}-Ben pigment at ϕ values of 0.05 and 0.2 respectively. In both cases E_{corr} values over the intact coating surface (E_{intact}), along with E_{corr} values measured at the defect-coating edge remained similar to the unpigmented case. However, corrosion driven delamination rates were found to be reduced and the extent of rate reduction was found to increase with pigment volume fraction ϕ. The E_{corr} vs. distance profiles obtained at $\phi = 0.05$ are distinguished by a significantly greater cathodic polarisation at the delamination front than previously observed in the absence of pigment. From figure 4a, a 0.35V potential drop is observed at the delamination front, while the gradient of the potential drop linking the cathodic front to the defect appears to decrease with time from 0.12 V mm^{-1} at 240 min, to 0.038 V mm^{-1} after 24 h. For the higher ϕ Ben-Ca^{2+}-containing coating, it may be seen that the boundary between the sharp delamination front E_{corr} drop and the more gradual linear potential gradient linking to the defect region becomes blurred so that the E_{corr} - distance gradient increases smoothly from defect to delamination front. For comparison, E_{corr} - distance profiles recorded for a commercially available $SrCrO_4$ pigmented PVB coating on Fe at $\phi = 0.05$ under identical conditions are given in Figure 5. In contrast to the E_{corr} profiles observed for Ben-Ca^{2+}-pigmented coatings, the sharp E_{corr} drop marking the position of the delamination front becomes indistinguishable from the disbonded region only after delamination has

initiated and the cathodic front has progressed several mm distant from the coating defect. Another difference observed for the $SrCrO_4$ pigmented case is that the gradient of the E_{corr}-distance plot remains constant at ca 0.14 V mm^{-1}, regardless of the distance moved by the disbondment front. In addition, E_{corr} values observed near the defect are ca. 0.1V higher than typically observed in the presence of $SrCrO_4$, signifying that some underfilm passivation may be occurring as CrO_4^{2-} is released into the thin electrolyte layer ingressing beneath the delaminated coating. Figures 6 a and b show plots of the time-dependent distance (from the defect edge) over which delamination has occurred (x_{del}) versus $(t_{del} - t_i)^{1/2}$, for Ben-Ca^{2+} and $SrCrO_4$ pigmented coatings respectively where t_{del} is the electrolyte contact time and t_i is the time taken for delamination to become initiated. Each curve in Fig. 6 was obtained for a different ϕ value, including for comparison the unpigmented case where ϕ = zero (curve i in both Fig. 6a and 6b). For the Ben-Ca^{2+} case (Fig 6a) it may be seen that delamination rates decrease progressively with increasing ϕ, indicating a progressive inhibition of corrosion-driven coating disbondment, but remain non-zero even when $\phi = 0.2$. However, the parabolic rate plots in Fig. 6a remain substantially linear over the $0 \leq \phi \geq 0.2$ range studied, indicating that the rate limiting step of the cathodic disbondment process remains unchanged even in the case of highly inhibited coating. Previous work on uninhibited coated iron has shown that overall rate of delamination is controlled by the migrational mass transport of electrolyte cations (Na^+ (aq) in this case) across the delaminated zone of the delamination of the cell [10] which in turn gives rise to the observed that the parabolic kinetics. In direct contrast, Figure 6b shows that the in-coating $SrCrO_4$ significantly modifies the kinetics of the delamination process and straight line x_{del} versus $(t_{del} - t_i)^{1/2}$ plots are observed only in the case of $\phi \geq 0.022$. At higher ϕ values, considerable deviation from linearity is observed, where the forward progress of the disbondment front slows markedly and in some cases becomes halted completely at protracted holding times. A summary of the influence of ϕ on delamination rate, which compares the in-coating performance of both Ben-Ca^{2+} and $SrCrO_4$ inhibitive pigments on iron is given in Figure 7. In the case of $SrCrO_4$ (Fig 7, curve ii), where a deviation from linearity is observed at higher ϕ, kdel values are determined over the initial 12h of the delamination experiment where x_{del} versus $(t_{del} - t_i)^{1/2}$ plots exhibit a substantially linear relationship. Again the similarity of plots i and ii demonstrates the promise of the environmentally acceptable Ben-Ca^{2+} pigment as a Cr(vi) replacement for the protection of organic coated iron from failure via a cathodic disbondment mechanism.

Further experiments were carried out in order to determine the possible contribution to the overall inhibition mechanism of in-coating inhibitor ions released into the defect electrolyte. In this scenario, Ca^{2+} cations stored in the bentonite pigment would exchange with Na^{+} cations (from the corrosive NaCl (aq) electrolyte applied to the defect region) in the vicinity of the coating-defect interface. Subsequent corrosion inhibition occurring on the electrolyte covered bare Fe would therefore be expected to influence to the overall localised delamination cell to a certain degree. In order to determine the effect of Ca^{2+} cation released into the defect electrolyte layer, varying quantities of $CaCl_2$ were dissolved in the 0.86 mol dm^{-3} aqueous experimental electrolyte. Figure 8 shows x_{del} versus $(t_{del} - t_i)^{1/2}$ plots obtained using unpigmented PVB coatings when the experimental electrolyte contained zero, 0.01 and 0.1 mol dm^{-3} $CaCl_2$. It may be seen from that external Ca^{2+} cations do reduce delamination rates slightly, but that even when $CaCl_2$ = 0.1 mol dm^{-3} the delamination rate remains *ca.* 10 times that obtained using the Ca^{2+} pigment at $\phi = 0.2$. The same type of experiment was also carried out to ascertain the influence of CrO_4^{2-} ions leaching from the sparingly soluble $SrCrO_4$ pigment into the NaCl (aq) electrolyte at the defect-coating boundary. To this end, solid $SrCrO_4$ was dispersed within an aliquot of 0.86 mol dm^{-3} aqueous NaCl solution and stirred for 5 min, whereupon the suspension was allowed to settle and the clear supernatant, containing ca 3×10^{-3} mol dm^{-3}, [12] was applied to the defect region of a PVB coated Fe delamination specimen.

A comparison of delamination kinetics of the unpigmented PVB-coated iron in the presence and absence of saturated $SrCrO_4$ is also given in Figure 4 (curves iv and i respectively). The presence of dissolved CrO_4^{2-} again only marginally slows down the rate of delamination, with k_{del} reduced from 0.55 to 0.35 mm $min^{-1/2}$. Parabolic kinetics was observed for both Ca^{2+} and CrO_4^{2-} inhibited defect electrolytes. The observations are in broad agreement with previous published observations on PVB coated galvanised steel [12,17,18], where inhibitor species added to the experimental electrolyte, including dissolved CrO_4^{2-} [12] were far less effective than in-coating inhibitive pigments in slowing corrosion-driven delamination. The lack of efficiency for CrO_4^{2-} may be understood in terms of the exclusion of external anionic species from entering the thin electrolyte layer within the disbonded region, where net negative charge is produced at the underfilm cathode. In contrast, Ca^{2+} cations added to the external electrolyte will co-migrate with Na^{+} into the underfilm region, but the hydrolytic instability of Ca^{2+} will cause solid $Ca(OH)_2$ to precipitate as a counter-current of OH^{-} anions is encountered. The fact

increasing the Ca^{2+} concentration from 10^{-2} to 10^{-1} mol dm^{-3} in the external electrolyte causes a small decrease in k_{del} from 0.42 to 0.32 mm $min^{-1/2}$ suggests that Ca^{2+} cations released into the defect play a relatively minor role in the overall inhibition process, compared to in-coating Ca^{2+} exchanged directly into the underfilm region.

3.2 Inhibition of coating failure by an anodic disbondment mechanism

It has been demonstrated elsewhere [27], that under a situation where a significantly reduced concentration and volume of aqueous NaCl is employed in order to initiate underfilm corrosion, then organic coating failure by an anodic disbondment (filiform corrosion) mechanism can occur. Preliminary experiments were conducted to ascertain whether in-coating Ben-Ca^{2+} and $SrCrO_4$ pigments were effective in inhibiting both the initiation and propagation of corrosion filaments on iron. As described in section 2, coated iron specimens were prepared using PVB containing dispersed Ben-Ca^{2+} and $SrCrO_4$ at $\phi = 0.15$, along with unpigmented PVB as a control. Following initiation of underfilm corrosion by application of a fixed volume (2 μL) or 0.01 mol dm^{-3} to a penetrative 2 mm long defect scribed in the centre of the PVB coated substrate, specimens were maintained at 95% relative humidity and room temperature for a period of up to 160 h. In the case of unpigmented PVB, repetitive SKP scans showed that underfilm corrosion propagated by in two distinct phases. Typical time-dependent interpolated grey-scale E_{corr} maps, recorded at various times during a 10 day in-situ experiment are given in Figure 9. It can be seen that initially the intact , uncorroded PVB coated iron surface exhibits an E_{corr} value of approximately +0.1 - +0.15V vs SHE, consistent with a substantially passive state. However, a SKP scan taken only 4h following application of the NaCl (aq) initiating electrolyte shows a significant radial de-passivated zone surrounding the penetrative coating defect (fig 9a), caused by a corrosion driven cathodic disbondment process. Subsequent scans, typified by Fig 9b, showed that the expansion of this depolarised region continued up to a period of ca. 50 h following initiation, where the delaminated zone extended beyond the boundaries of the 1 cm^2 scan area . As the radial growth of this zone ceased, areas of focal anodic activity (E_{corr} = ca –0.2 V vs SHE) located in the vicinity of the central defect started to fragment. These areas, comprising the active electrolyte-filled heads of corrosion filaments, propagated away from the defect region, travelling within the delaminated region at a velocity of 0.38 ± 0.02 μm min^{-1}. Behaviour is typified by Fig 9c, where the two small circular regions of 0,5 mm diameter, *ca.* 2.5 mm to both the left and right

hand sides of the central defect, comprise the corrosion filament heads. These, along with their associated tails of dried iron oxide corrosion product are clearly visible in Fig 9d, which shows the physical appearance of the scanned area 160h following corrosion initiation.

In contrast, the $SrCrO_4$-pigmented coating showed minimal evidence of underfilm corrosion surrounding the scribe, even after 160 h exposure to a 95% relative humidity environment. However, under the same conditions the Ben-Ca^{2+} inhibited specimen did suffer a certain degree of cathodic disbondment following initiation of underfilm corrosion. Over the first 36h of exposure to 95% rh, a radial cathodically disbonded region extending ca 2 mm from the defect was observed, as shown in Figure 10a. At longer holding times, the growth of this delaminated zone was halted (see Figure 10b), though filiform corrosion was observed to initiate in the vicinity of the penetrative scribe and subsequently propagate within the radial delaminated zone. After 160h, several of the filaments had lengthened to the extent that they propagation into the previously intact organic-coated region. A mean filament velocity of 0.44 $\pm$ 0.05 $\mu m\ min^{-1}$, measured for filaments propagating in the previously cathodically-disbonded region, decreased to 0.33$\pm$ 0.05 $\mu m\ min^{-1}$ for those extending into the previously intact region. The occurrence of significant filiform corrosion was confirmed by the visual appearance of the Ben-Ca^{2+} inhibited specimen at the end of the experiment (see Figure 10d). From these results it is evident that Ben-Ca^{2+} inhibitive pigments are ineffective at forestalling underfilm corrosion of organic-coated iron involving an anodic (filiform) disbondment corrosion mechanism.

4. Discussion

4.1 Bentonite pigments

Bentonite clays are a form of montemorillonite and exhibit intrinsic cation exchange properties, which are substantially independent of pH. Montemorillonites are 2:1-layer hydrated aluminium silicates based on the dioctahedral pyrophyllite structure [15]. The pyrophyllite structure consists of extended two-dimensional sheets or layers, each consisting of annellated cyclic groups of silicate tetrahedra flanking octahedrally coordinated aluminium (hydr)oxide groups. In montemorillonite, partial isomorphous substitution of magnesium (II)

for aluminium (III) occurs in the octahedral layer, resulting in a net anionic charge of 0.67 units per unit cell. Anionic layer charge arises from incomplete neutralisation of the negative charge on the apical oxygens and on groups coordinated to magnesium. Thus, an ideal montemorillonite may be defined as having the unit cell composition,

$$[(Si_8)^{tetrahedral} \bullet (Al_{3.33}\, Mg_{0.67})^{octahedral} \bullet O_{20}\,(OH)_4]\ 0.67M^+ \qquad (2)$$

where M^+ represents a univalent charge compensating cation. Most native montemorillonites, or bentonites, have compositions similar to formula (2) but may contain additional isomorphous substitution; e.g. iron (III) for aluminium (III) or aluminium (III) for silicon (IV).

The charge compensating cations, M^+ in formula (2), are not part of the montemorillonite layer structure. Instead they exist as freely exchangeable species, intercalated between aluminosilicate sheets. The nature of the exchangeable cation depends on the origin of the clay. Wyoming bentonites and Texas bentonites tend to have Na^+ and Ca^{2+} as the principal exchangeable cations, respectively. However, these cations may be rapidly exchanged in the laboratory by passing a suspension of bentonite through a cation exchange column or by repeatedly washing the bentonite with a solution containing the desired cation. The interaction between sheets and exchangeable cations is purely electrostatic and osmotic forces may cause montemorillonites to swell on contact with water. The degree of swelling decreases markedly with the valence of the exchangeable cation. Thus, monovalently exchanged (e.g. Na^+) montemorillonites swell dramatically and may become fully delaminated at low ionic strengths. Whereas, divalently (e.g. Ca^{2+}) and trivalently (e.g. Ce^{3+}) exchanged montemorillonites exhibit only very limited swelling. Consequently, the alkaline earth and rare earth exchanged bentonites used here may be regarded as dimensionally stable (substantially non-swelling), pH neutral, inorganic pigments.

4.2 Inhibition of cathodic disbondment

It has been shown elsewhere that during corrosion driven cathodic coating delamination cathodic O_2 reduction, reaction (3), occurs primarily in the region of the delamination front. Conversely, anodic metal dissolution, reaction (4), is constrained to the region of the coating defect.

$$O_2 + 2H_2O + 4e^- \longrightarrow 4OH^- \quad (3)$$

$$Fe \longrightarrow Fe^{2+} + 2e^- \quad (4)$$

Ionic current passes along the thin layer of electrolyte, which becomes ingressed beneath the delaminated coating, to link the cathodic and anodic processes. It has also been shown that in the absence of inhibition this ionic current, and hence the rate of delamination, is limited by the migrational mass transport of cations (in our case Na^+) from the external electrolyte to the delamination front. Thus, in Fig. 1, the sharp potential drop at the delamination front may be understood to arise from the ingress of ions, loss of coating adhesion, and the onset of reaction (3). Similarly, potentials in the defect region ultimately approximate those anticipated for the reaction (4) equilibrium potential, *i.e.* -0.44 V *vs.* SHE. The approximately linear potential gradient linking the defect and delamination front regions arises ohmically as a consequence of the finite ionic conductivity of the underfilm electrolyte layer. Overall rate control by cation migration in this electrolyte layer gives rise to the parabolic delamination distance-time relationship seen in the data for unpigmented PVB coatings shown in Figs. 2 and 6.

The influence of Ca^{2+} exchanged bentonite pigment on the corrosion delamination cell is illustrated in figures 4a and 4b. The decreasing delaminated region potential gradient (dE/dx) observed with time for ϕ (Ben-Ca^{2+}) = 0.05, shown in figure 4a, suggests a gradual decrease in the magnitude of ionic current with time, assuming the underfilm conductivity remains constant. In fact, any occurrence of underfilm exchange of Na^+ with hydrolytically unstable Ca^{2+} ions should work to decrease underfilm conductivity and thus give rise to a greater potential gradient for a given ionic current. Fig 4b shows that when ϕ (Ben-Ca^{2+}) = 0.2, the sharp change in $E_{corr}(x)$ gradient at the delamination front – ohmic region boundary has become blurred by comparison to the unpigmented case seen in Fig 1. Such a change is consistent with a decrease in electrolyte conductivity in the underfilm electrolyte layer near the delamination front, giving rise to an increased ohmic potential gradient. If a reduction in underfilm electrolyte conductivity is also responsible for the observed reduction in delamination rate it follows that the delamination kinetics will remain controlled by underfilm cation migration when Ca^{2+} pigment is present. This hypothesis is consistent with fig. 6a,

which shows that whilst delamination rates decrease by over an order of magnitude with increasing Ca^{2+} pigment volume fraction, the x_{del} *vs.* $(t_{del} - t_i)^{1/2}$ plots remain linear even at ϕ = 0.2. Because similar trends in delamination rate and similar x_{del} vs. $(t_{del} - t_i)^{1/2}$ relationships were observed for all the cation exchanged bentonite pigments is reasonable to assume that these all function in a similar way, *i.e.* by decreasing the conductivity of the underfilm electrolyte layer.

If we consider Na^+ cations migrating in the delamination cell electric field from the external electrolyte to the delamination front along the underfilm electrolyte layer, these will continually encounter particles of bentonite pigment as they pass beneath the delaminated coating. It may be understood that this situation resembles the passage of electrolyte through an ion-exchange column. The underfilm electrolye layer is very thin (typically < 5 μm) [11] so that lateral diffusion of cations need only occur over short distances. Consequently, cation exchange will be efficient when ϕ values are large. Thus, for ϕ > the critical percolation volume fraction *ie. ca.* 0.15 we may expect practically all the underfilm Na^+ to become exchanged by Ca^{2+}. Furthermore, the production of OH^- by reaction (3) results in highly alkaline underfilm pH, typically > pH 10.[11] Indeed, several authors have reported that the underfilm pH encountered for cathodic blisters formed on steel can be as high as pH 14.[28,29] It is therefore likely that Ca^{2+} cations will be precipitated as the solid, electrically non-conductive, hydroxide $Ca(OH)_2$, resulting in sharply reduced underfilm conductivity. At lower ϕ values ion-exchange will be less complete and underfilm conductivity will be higher, producing the delamination rate - ϕ relationship seen in figures 6a and 7. The notion that the degree of ion exchange determines the level of inhibition is also supported by these results. The mobilities of Na^+ and Ca^{2+} are similar to the extent that their concentration ratio in the underfilm electrolyte layer will approximate that found in the external electrolyte. Fig. 8 therefore implies that delamination rates fall progressively with increasing underfilm Ca^{2+}/Na^+ concentration ratio. Exactly similar arguments may be used to explain coating delamination inhibition by all the other cation exchanged bentonites.

Underfilm cation exchange was confirmed by imaging SIMS analysis of an iron substrate previously coated using Ca^{2+}-Ben bearing PVB at ϕ = 0.2, as described in the experimental section. 48h after initiation of corrosion and incubation at 96% rh, the coating was carefully peeled away and a portion of the iron surface encompassing the clearly visible delaminated

zone, extending radially some 3mm beyond the coating defect, was subjected to chemical analysis (schematically illustrated in Figure 11a). A secondary electron image together with calcium and sodium elemental maps are shown in Figs. 11 b, c and d respectively. A clear demarcation is observed between the cathodically delaminated zone (seen on the right in Fig 11b as slightly lighter than the background) and the sample area previously covered with an intact coating. Figure 11c shows that large areas of the delaminated zone, especially a 1 mm strip immediately to the right of the apparent delamination front are abundant in calcium ions. Conversely Fig 11d shows that the areas of high sodium abundance do not correspond to locations on the surface which are rich in Ca^{2+} deposits. Interestingly, a thin line of high Na^{+} abundance appears to coincide with the position of the delamination front marked in fig 11a, suggesting that although effective exchange of Na^{+} by Ca^{2+} occurs in the delaminated zone itself, there is little evidence of this occurring at the point where cathodic oxygen reduction is at its maximum level.

If we assume that cationic strength in the underfilm layer is a value similar to that present in the external electrolyte, *i.e.* 0.86 mol dm^{-3}, then the minimum pH at which metal hydroxide precipitation will first occur may be calculated as shown in Table 1. It may be seen that $Ce(OH)_3$, $Y(OH)_3$ and $Mg(OH)_2$ are all highly insoluble, first precipitating at near neutral pH. Conversely, $Ca(OH)_2$, $Sr(OH)_2$ and $Ba(OH)_2$ are more soluble, requiring a minimum precipitation pH > 10. However, comparison with fig. 3 shows that it is those cations with more soluble hydroxides that provide the more efficient inhibition. Possibly this is due to cation exchange efficiency becoming compromised by hydroxide precipitation on or near the bentonite particles in the case of the less soluble hydroxides. Under normal atmospheric conditions the precipitated hydroxides would become converted to carbonates by reaction with ambient CO_2 so that, ultimately, carbonate solubility would be more important than hydroxide solubility. However, the fact that our experiments were conducted under conditions where the ingress of laboratory air was extremely limited suggests that it is the hydroxides themselves that are responsible for the inhibition reported here. Certainly, the failure of the unexchanged (native) Wyoming bentonite to inhibit coating delamination, as seen in Fig. 3, confirms that it is the nature of the exchangeable cations and the species derived from them, and not the bentonite itself, which is responsible for inhibition of coating delamination. The underfilm processes responsible for the inhibitive nature of in-coating group II-exchanged bentonite pigments are summarised schematically in Figure 12.

The comparison of delamination rate constant versus ϕ relationships for both Ben-Ca^{2+} and $SrCrO_4$-show a similar efficiency of inhibition, although the variation in the shape of kinetic plots in Figures 6a and b suggests significantly differing inhibition mechanisms. In previous studies of the inhibition of cathodic disbondment on the zinc surface of galvanised steel by in-coating $SrCrO_4$ pigment [12], it was proposed that the most significant factor in decreasing delamination comprised the replacement of under-film O_2 reduction by a self-limiting CrO_4^{2-} reduction process, represented by equation (5), with an associated pH dependent electrode potential given by equation (6). [30]

$$CrO_4^{2-}{}_{(aq)} + 5H_2O + 3e^- \rightleftharpoons Cr(OH)_{3(s)} + 5OH^- \quad (5)$$

$$E^o = 1.244 - 0.988pH + \log[CrO_4^{2-}] \quad (6)$$

The hydrolysis of the Cr(iii) species produced at elevated pH to give a solid hydroxide, which rapidly blocks off further cathodic activity on the original underfilm site of reaction (3) is represented schematically in Figure 13. Strong evidence for this proposed theory involving a self-limiting CrO_4^{2-} reduction reaction is obtained from the SKP-derived kinetic plots of time-dependent delamination distance given in Figure 6b, where a transition from an ohmically limited process at low ϕ to a different rate determining step, probably related to the stifling of cathodic underfilm oxygen reduction, is suggested by the deviation from linearity obtained at higher $SrCrO_4$ pigment loadings.

The difference in behaviour between the two pigment types is also evident in the comparison of efficiency for the inhibition of coating failure under more realistic circumstances, discussed in section 3.2, where both cathodic and anodic modes of disbondment are present. In this scenario, where a significantly lower quantity of initiating NaCl is employed, the $SrCrO_4$ pigment clearly out-performs the Ca^{2+}-Ben. While the presence of in-coating Ca^{2+}-Ben again slows an initial cathodic disbondment phase, a significant extent of filiform corrosion is seen to affect regions of the coated surface in the vicinity of the penetrative coating defect (see Fig 10b and c). In addition, the presence of Ca^{2+}-Ben has little effect in slowing the progress of individual filament once they have initiated and measured velocities were similar to those established on an unpigmented PVB-coated iron surface. The low inhibition efficiency of in-coating exchangeable Ca^{2+} cations can be explained in terms of the chemistry of the local corrosion cell in filiform corrosion. As mentioned at length

elsewhere [31,32,33], the principal driving force for corrosion filament propagation is considered to be differential aeration, where anodic dissolution of iron, according to reaction (4), is located at the oxygen-deficient leading edge of the electrolyte-filled filament head. Rapid oxygen transport through a tail of dry, porous corrosion product produces a net oxygen cathode (reaction 3) at the rear of the head. Although bentonite pigments can sequester some H^+ and Fe^{2+} cations from the filament head electrolyte, with the concomitant release of stored Ca^{2+} cations, the limited exchange capacity of the pigment results in an exchange efficiency of significantly less than 100%. To inhibit filament propagation, Ca^{2+} cations released into the acidic anterior of filament heads must migrate to the local cathode at the rear of the head in order to precipitate solid hydroxide at sites of oxygen reduction. Although the pH in this region will be higher than at the front of the head, it will be considerably lower than the threshold value (see Table 2) required to precipitate a film of solid $Ca(OH)_2$. This therefore explains why rates of corrosion filament propagation on Ben-Ca^{2+} coated iron samples remain similar to those measured for unpigmented coatings. In contrast, the presence of SrCrO4 at the same pigment volume fraction inhibits even the initiation of filiform corrosion. This is turn suggests that CrO_4^{2-} anions leaching into the NaCl electrolyte applied to the scribe have a sufficiently powerful inhibitory effect to limit the generation of the underfilm low pH, Fe^{2+}-rich electrolyte capable of causing corrosion filaments to initiate. In this respect the observations made on PVB coated iron closely resemble those made previously for $SrCrO_4$ [34] and smart release bentonite [35] inhibited coatings applied to AA2024 aerospace alloy.

Conclusions

Wyoming bentonite clay pigments exchanged with Ca^{2+}, Sr^{2+}, Ba^{2+}, Mg^{2+}, Ce^{3+} and Y^{3+} cations have been shown to significantly enhance resistance to corrosion-driven cathodic delamination in organic coatings adherent to iron surfaces. The dependence of coating delamination rate on Ca^{2+} bentonite pigment volume fraction has been determined and shown to be comparable with that for a conventional strontium chromate ($SrCrO_4$) pigment. For all the cation exchanged bentonites, coating delamination rates decrease progressively with increasing pigment volume fraction. However, the delamination kinetics remain consistent with overall rate control by underfilm cation migration even when inhibition is profound. An inhibition mechanism has therefore been proposed whereby underfilm cation exchange and the precipitation of sparingly soluble hydroxides reduces underfilm electrolyte conductivity.

Paradoxically, cations with more soluble hydroxides such as Ca^{2+}, Sr^{2+}, Ba^{2+} give better inhibition than cations with less soluble hydroxides such as Mg^{2+}, Ce^{3+} and Y^{3+}. Possibly this is due to precipitation of less soluble hydroxides at or near the bentonite surface compromising further cation exchange. The fact that naturally Ca^{2+} exchanged Texas bentonites are cheaply available suggests that Ca^{2+} bentonite pigments are worthy of further technological evaluation. However, as a final note of caution, it should be noted although promising results were obtained in slowing organic coating failure by cathodic disbondment, the same efficiency did not extend to the inhibition of filiform corrosion.

Figure Legends

Figure 1: Plots of time-dependent E_{corr} versus distance profiles for a 30 μm unpigmented PVB coating applied to an iron substrate. The electrolyte in contact with the defect is 0.86 mol dm^{-3} NaCl (aq). Time key: curve i = 90 min, ii, iii… at 60 min intervals thereafter.

Figure 2: SKP-derived E_{corr} versus distance profiles for a PVB coating containing dispersed Y^{3+}-Ben pigment at a volume fraction (ϕ) of 0.15, applied to an iron substrate. The electrolyte in contact with the defect is 0.86 mol dm^{-3} NaCl (aq). Time key: curve i = 2h, ii 4h, iii, vi etc at 3h intervals thereafter. The inset shows a comparison of delamination distance (x_{del}) versus $t^{1/2}$ plots obtained in the presence and absence of pigment.

Figure 3: Comparison of delamination rates obtained for various PVB-based coatings containing various inhibitor pigments applied to iron using ϕ = 0.15. NB. none signifies that no pigment is present.

Figure 4: Plots of time-dependent E_{corr} versus distance profiles for PVB coatings containing dispersed Ca^{2+}-Ben pigment at volume fraction (ϕ) of (a) 0.05 and (b) 0.2 applied to an iron substrate. In both cases the electrolyte in contact with the defect is 0.86 mol dm^{-3} NaCl (aq). Time key (a) curve i = 2h, ii, iii, iv and v at 2h intervals and vi, vii and viii at 4 hourly intervals. (b) curve i = 2h, ii 4h, and iii, vi 6 hourly intervals.

Figure 5: Plots of time-dependent E_{corr} versus distance profiles for a $SrCrO_4$-pigmented PVB coating on iron at a pigment volume fraction ϕ of 0.1. The electrolyte in contact with the defect is 0.86 mol dm^{-3} NaCl (aq). Time key: curve i = 2h, ii =3h, iii = 5h min, iv = 7h v = 10h and at 5h intervals.

Figure 6: Delamination kinetics plotted for a series of (a) Ca^{2+}-Ben and (b) $SrCrO_4$ pigmented PVB coatings applied to iron substrates. In each case the electrolyte in contact with the defect is 0.86 mol dm^{-3} NaCl (aq). Ca^{2+}-Ben (a): plots of x_{del} versus $(t_{del} - t_i)$ are shown for pigment volume fractions (ϕ) of i. 0, ii. 0.02, iii. 0.05, iv. 0.1, v. 0.15 and vi. 0.2. $SrCrO_4$ (b): x_{del} versus $(t_{del} - t_i)$ plots are shown for ϕ = i. 0, ii. 0.011, iii. 0.022, iv. 0.035, v. 0.049, vi. 0.081 and vii. 0.11.

Figure 7: Plots of delamination rate constant (k_{del}) as a function of pigment volume fraction ϕ for: i. Ca^{2+}-Ben and ii. $SrCrO_4$ pigmented PVB coatings on iron.

Figure 8: Plots of delamination distance (x_{del}) versus $(t_{del} - t_i)^{1/2}$ for unpigmented PVB coatings on iron. Electrolyte in contact with the defect is 0.86 mol dm^{-3} NaCl, i = uninhibited, ii = inhibited using 10^{-2} and iii. 0.1 mol dm^{-3} $CaCl_2$. Plot iv was obtained when the defect electrolyte was in contact with dispersed $SrCrO_4$ pigment, giving a saturated chromate concentration of 3×10^{-3} mol dm^{-3}.

Figure 9: Interpolated greyscale maps showing E_{corr} distributions measured over a PVB coated iron surface at times (a) 4, (b) 14 and (c) 160 h following initiation using 2 μL of 0.01 mol dm^{-3} NaCl (aq). (d) is a photographic image of the sample at the end of the experimental period.

Figure 10: Interpolated greyscale maps showing E_{corr} distributions measured over a Ca^{2+}-Ben pigmented (ϕ = 0.2) PVB coated iron substrate at (a) 36, (b) 130 and (c) 190 h following initiation using 2 μL of 0.01 mol dm^{-3} NaCl (aq). (d) is a photographic image of the sample at the end of the experimental period.

Figure 11: Cathodically delaminated iron surface imaged using SIMS microscopy 24 hours after initiation using 2 μL of 0.1%w/v NaCl (aq) and following the removal of the PVB +

Ca^{2+}-B (ϕ = 0.2) coating: **(a)** schematic illustration of sample area analysed, **(b)** secondary electron image **(c)** calcium distribution and **(d)** sodium distribution maps. The dotted arrow shows the extent of coating delamination.

Figure 12: Schematic representation of underfilm inhibition of corrosion-driven delamination occurring in the presence of in-coating Ben-Ca^{2+} pigment showing (a) underfilm cation exchange and (b) Ca (II) hydroxide precipitation at elevated pH.

Figure 13: Schematic representation of the inhibition of corrosion-driven cathodic delamination by an in-coating, sparingly soluble $SrCrO_4$ pigment.

Table 1. Solubilities of alkaline earth and rare earth hydroxides

Compound	**M_{sat} / M 25°C[b]**	**Log (K_s/M^3) 25°C**	**pH precipitate[c]**
$Ce(OH)_3$	---------	-19.9[a]	7.6
$Y(OH)_3$	---------	-22.1[a]	6.8
$Mg(OH)_2$	2.0×10^{-4}	-10.5[b]	8.9[b]
$Ca(OH)_2$	1.5×10^{-2}	-5.09[a]	11.7[a]
$Sr(OH)_2$	3.4×10^{-2}	0.45[a] -3.82[b]	14.4[a] 12.3[b]
$Ba(OH)_2$	1.5×10^{-1}	-2.98[a]	12.7[a]

a. Obtained from solubility product values in ref. [36].
b. Calculated from solubility values obtained in ref. [37].
c. Calculated assuming $n[M^{n+}] = 0.86$ mol dm^{-3}.

References

1. E.L. Koehler, Corrosion, **33**, (1977), 209.
2. H. Leidheiser and M.W. Kendig, Corrosion, **32**, (1979), 69.
3. J.S. Hammond. J.W. Holuka, J.E. DeVries and R.A. Dickie, Corros. Sci. **21**, (1981), 239.

4. H. Leidheiser and W. Wang, J. Coat. Technol. **53**, (1981), 77, Proc. Electrochem. Soc. **84**, (1984), 239.

5. J.J. Ritter, J. Coat. Technol. **54**, (1982), 51.

6. H. Leidheiser, L. Igetoft and W. Wang, Prog. Org. Coat. **11**, (1983)**,** 19.

7. E.L. Koehler, Corrosion, **40**, (1984), 5.

8. M. Stratmann, H. Streckel, and R. Feser, Corros. Sci. **32**, (1991) 467.

9. J.D.B. Sharman, J.M. Sykes and T. Handyside, Corros. Sci. **35**, (1993), 1375.

10. M. Stratmann, R. Feser, and A. Leng, Electrochim. Acta, **39**, (1994), 1207.

11. A. Leng, H. Streckel, and M. Stratmann, Corros. Sci. **41**, (1999), 579.

12. G. Williams and H. N. McMurray, J. Electrochem Soc. **148**, (2001), B337.

13. D. H. Solomon and D. G. Hawthorne, in Chemistry of Pigments and Fillers, Wiley, New York, (1983), p 1.

14. H. van Olphen, in An Introduction to Clay Colloid Chemistry 2nd. Edn., Wiley, New York (1977).

15. R. E. Grim, in Clay Mineralogy, McGraw-Hill, New York (1968).

16. S. Bohm, H. N. McMurray, S. M. Powell and D. A. Worsley, Materials and Corrosion, **52**, (2001), 896.

17. G. Williams, H.N. McMurray, D.A. Worsley, J. Electrochem. Soc. **149**, (2002), B154.

18. G. Williams, H.N. McMurray, M.J. Loveridge, Electrochim. Acta., **55**, (2010), 1740

19. B.R.W. Hinton, L. Wilson, Corros. Sci. **29**, (1989), 967.

20. D.R. Arnott, B.R.W. Hinton, N. E. Ryan, Mater. Performance, **26**, (1987), 211.

21. A.J. Aldykiewicz, A.J. Davenport, H.S. Isaacs, J. Electrochem. Soc. **143**, (1996), 147.

22. H.N. McMurray, S.M. Powell, D.A. Worsley, Corrosion, **55**, (1999), 1040.

23. S. Bohm, R. Greef, H. N. McMurray, D. A. Worsley, J. Electrochem. Soc. **147,** (2000), 3286.

24. K. Aramaki, Corros. Sci. **43**, (2001), 1573.

25. J. M. Adams *et al*. J. Catal. **58**, (1979), 238.

26. G. Williams, H.N. McMurray and D.A. Worsley, J. Forensic. Sci. **46**, (2001), 1085.

27. G. Williams and H.N. McMurray, Electrochem. Commun., **5** (2003), 871.

28. H. Leidheiser, Polymeric Materials for Corrosion Control, ACS 322 ,Washington D.C (1986).

29. J.J. Ritter and J. Kruger, Corrosion Control by Organic Coatings, NACE Publications: Houston, Texas (1981).

30. E. Deltombe, N. De Zoubov and M. Pourbaix, in Atlas of Electrochemical Equilibria in Aqueous Solutions, M. Pourbaix, Editor, p. 256, Pergamon Press, London (1966).
31. R.T. Ruggieri, T.R. Beck, Corrosion 39 (1983) 452.
32. A. Bauista, Prog. Org. Coat. 28 (1996) 49.
33. H.N. McMurray, G. Williams, 2.14 Under Film/Coating Corrosion, in: T.A.J. Richardson (Ed.), Corrosion in Liquids, Types of Corrosion in Liquids, Shreir's Corrosion, vol 2, fourth ed., Elsevier Ltd., 2009, p. 988.
34. H.N. McMurray, G. Williams, S. O'Driscoll, J. Electrochem. Soc. 151 (2004) B406.
35. G. Williams, H.N. McMurray, Electrochim. Acta, 69, (2012), 287.
36. M. Pourbaix, Editor, Atlas of Electrochemical Equilibria in Aqueous Solutions, Pergamon Press, London (1966), p 177.
37. R. D. Harrison, Editor, Chemistry and Physical Science book of Data, Longman Group, London (1972), p 64.

Figure 1

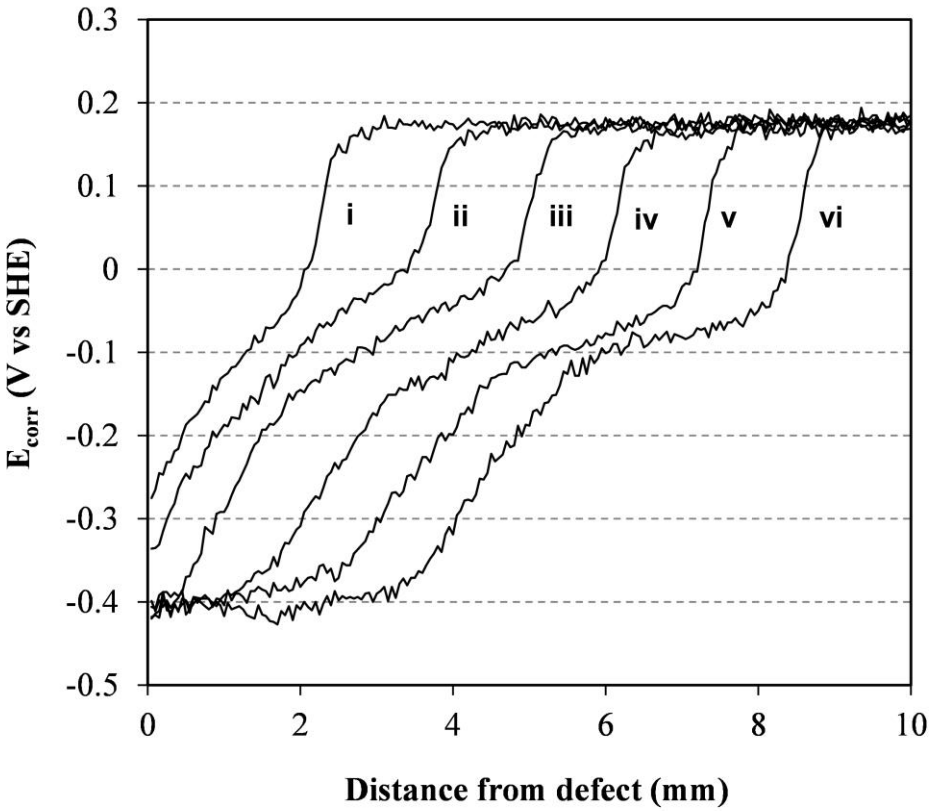
0.3
0.2
0.1
0
-0.1
-0.2
-0.3
-0.4
-0.5
0
2
4
6
8
10
i
ii
iii
iv
v
vi
E_corr (V vs SHE)
Distance from defect (mm)

Figure 2

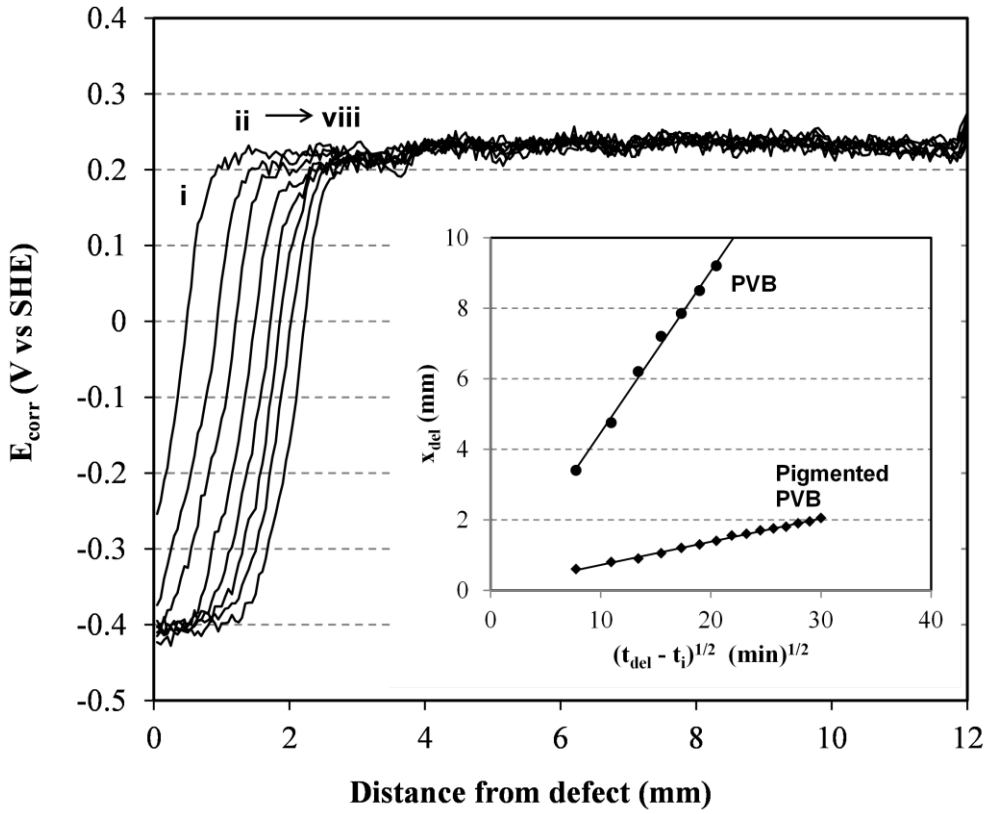
0.4
0.3
0.2
0.1
0
-0.1
-0.2
-0.3
-0.4
-0.5
0
2
4
6
8
10
12
ii → viii
i
E_{corr} (V vs SHE)
Distance from defect (mm)
10
8
6
4
2
0
0
10
20
30
40
x_{del} (mm)
$(t_{del} - t_i)^{1/2}$ $(min)^{1/2}$
PVB
Pigmented PVB

Figure 3

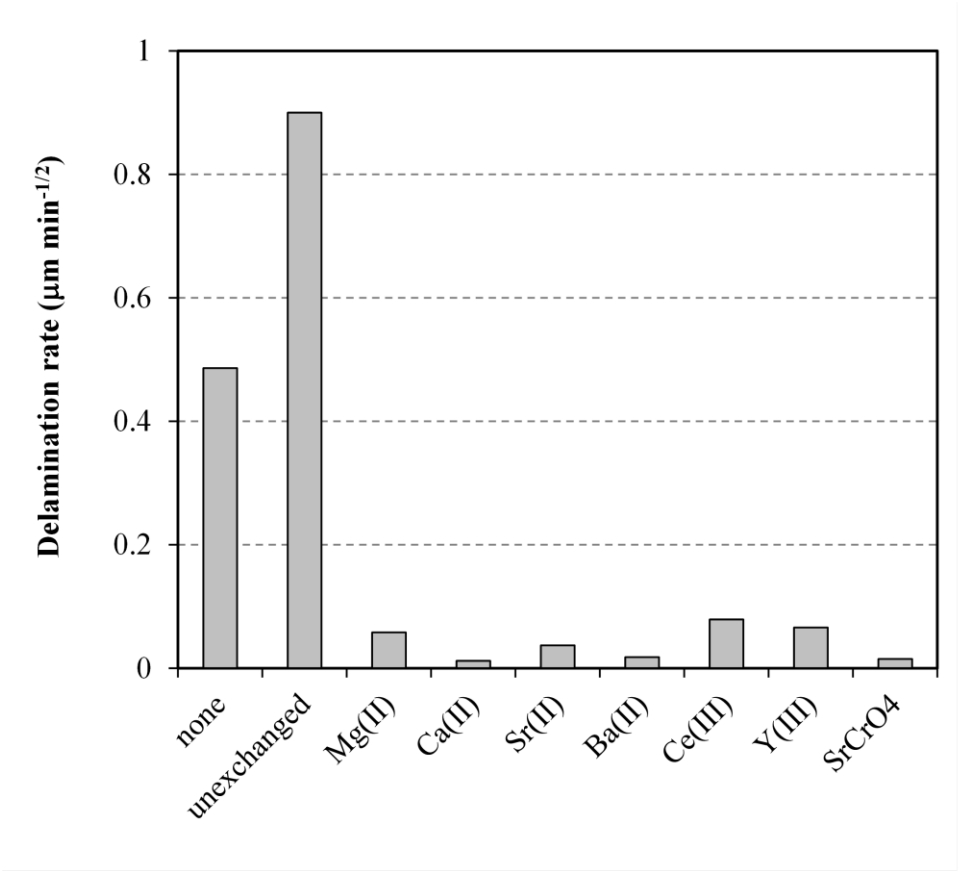
Delamination rate (µm min-1/2)
1
0.8
0.6
0.4
0.2
0
none
unexchanged
Mg(II)
Ca(II)
Sr(II)
Ba(II)
Ce(III)
Y(III)
SrCrO4

Figure 4a

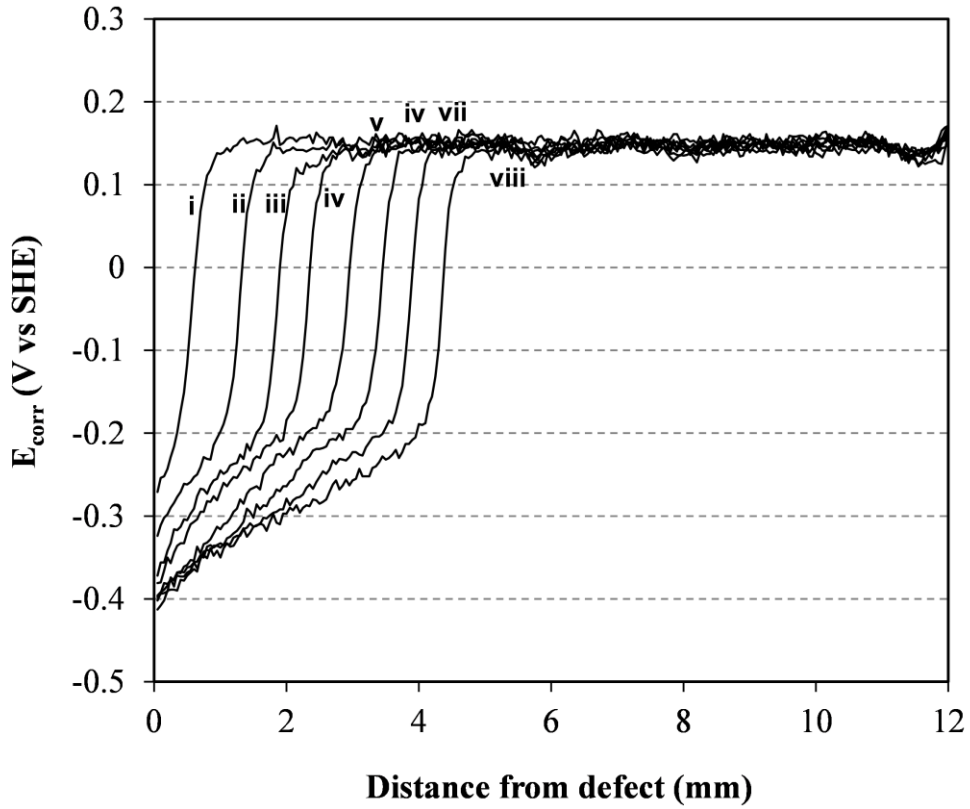
0.3
0.2
0.1
0
-0.1
-0.2
-0.3
-0.4
-0.5
0
2
4
6
8
10
12
E_{corr} (V vs SHE)
Distance from defect (mm)
i
ii
iii
iv
v
iv
vii
viii

Figure 4b

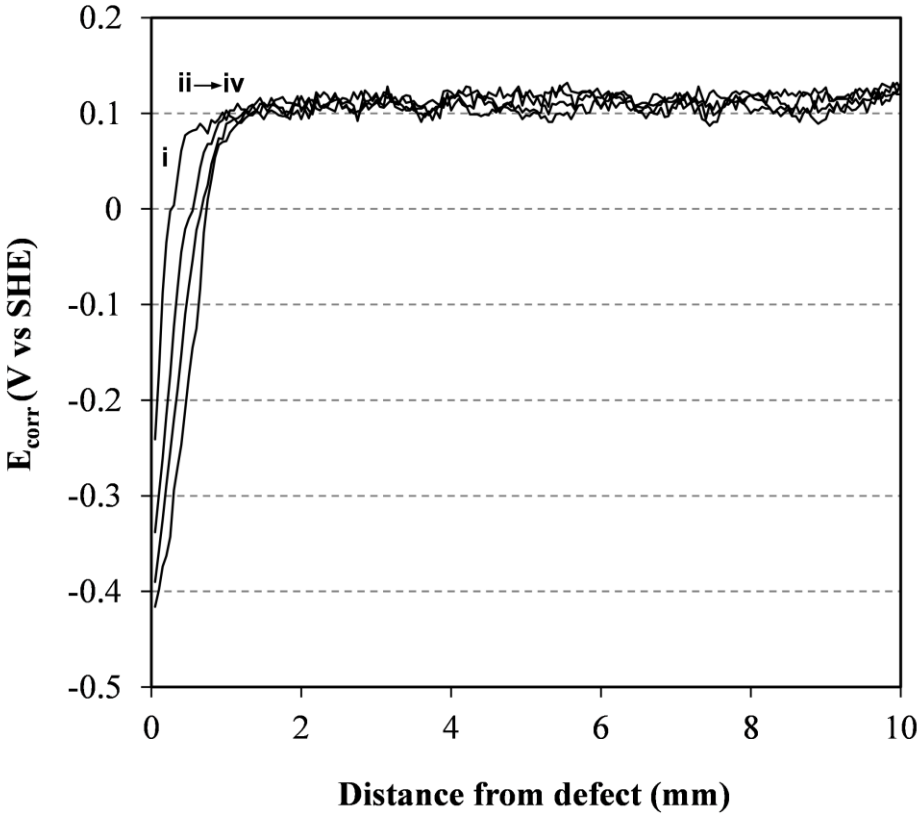
0.2
0.1
0
-0.1
-0.2
-0.3
-0.4
-0.5
ii→iv
i
E_{corr} (V vs SHE)
0
2
4
6
8
10
Distance from defect (mm)

Figure 5

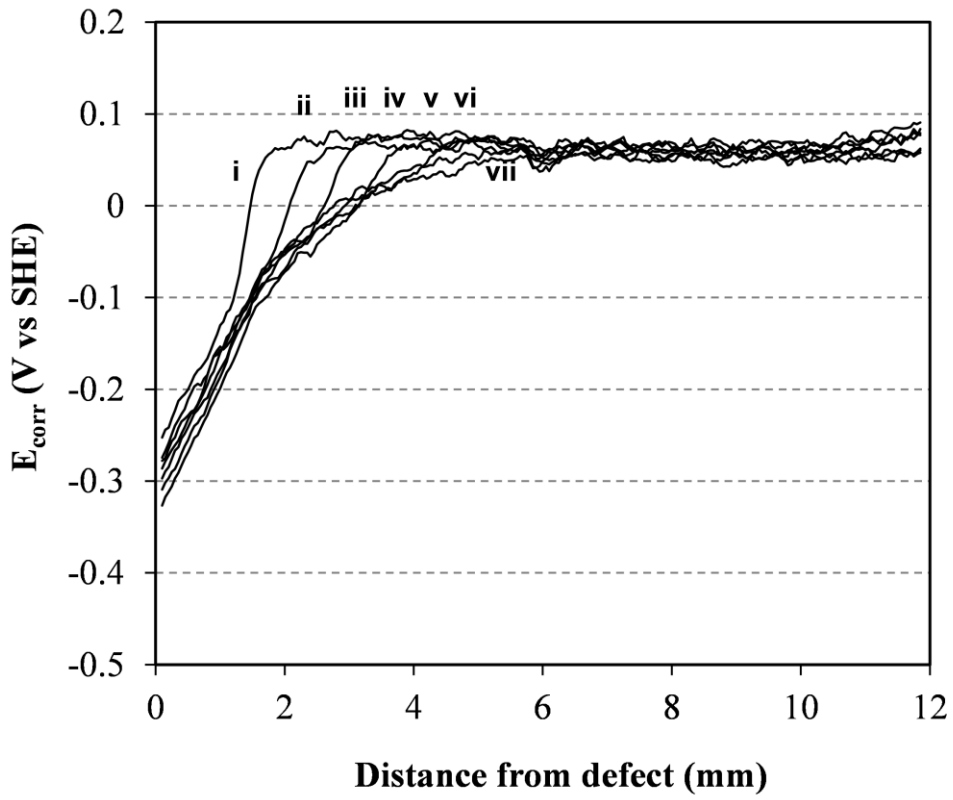
0.2
0.1
0
-0.1
-0.2
-0.3
-0.4
-0.5
0
2
4
6
8
10
12
i
ii
iii
iv
v
vi
vii
E_{corr} (V vs SHE)
Distance from defect (mm)

Figure 6a

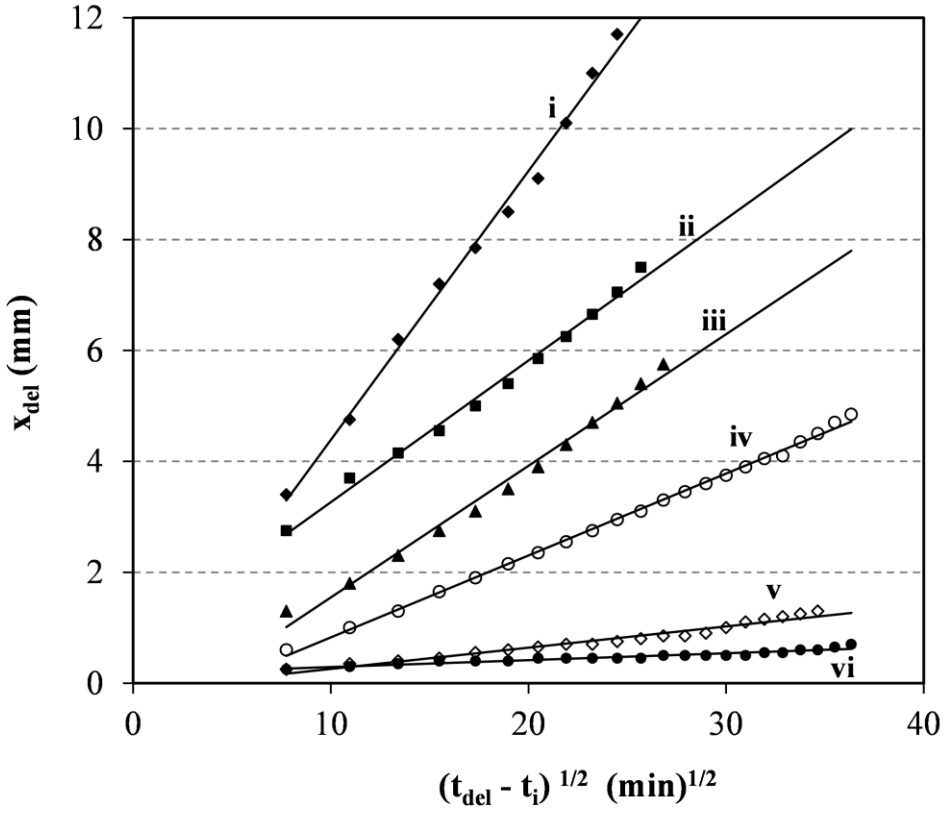

Figure 6b

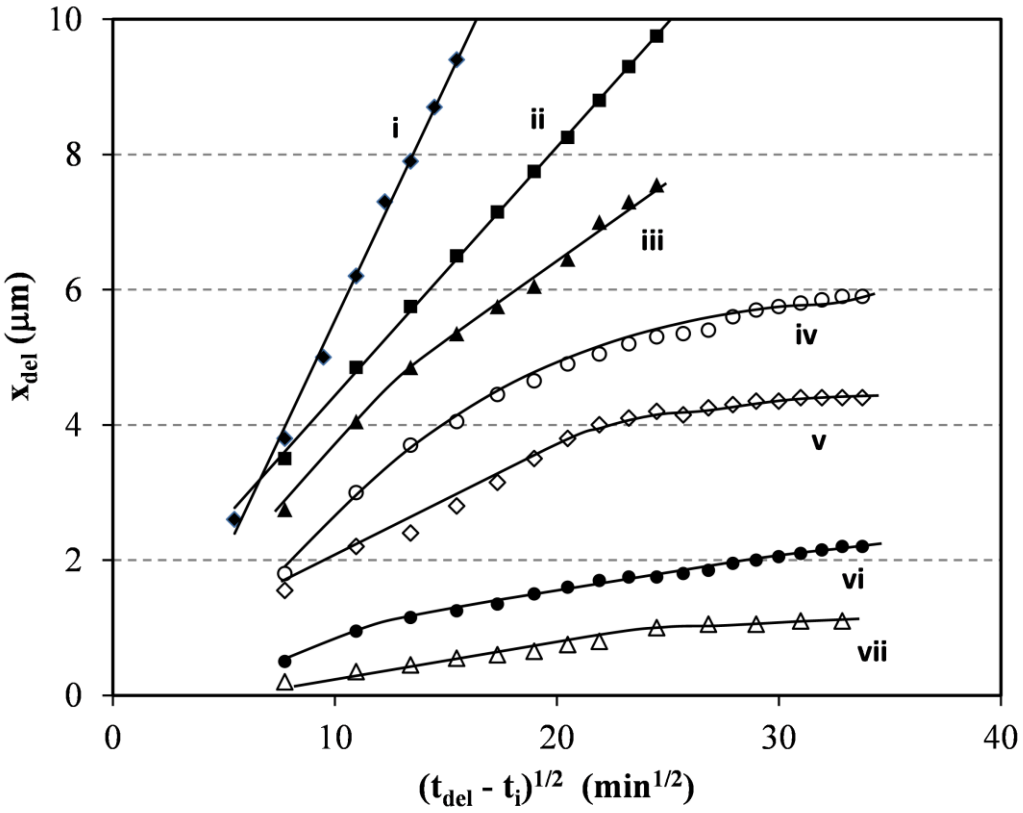

Figure 7

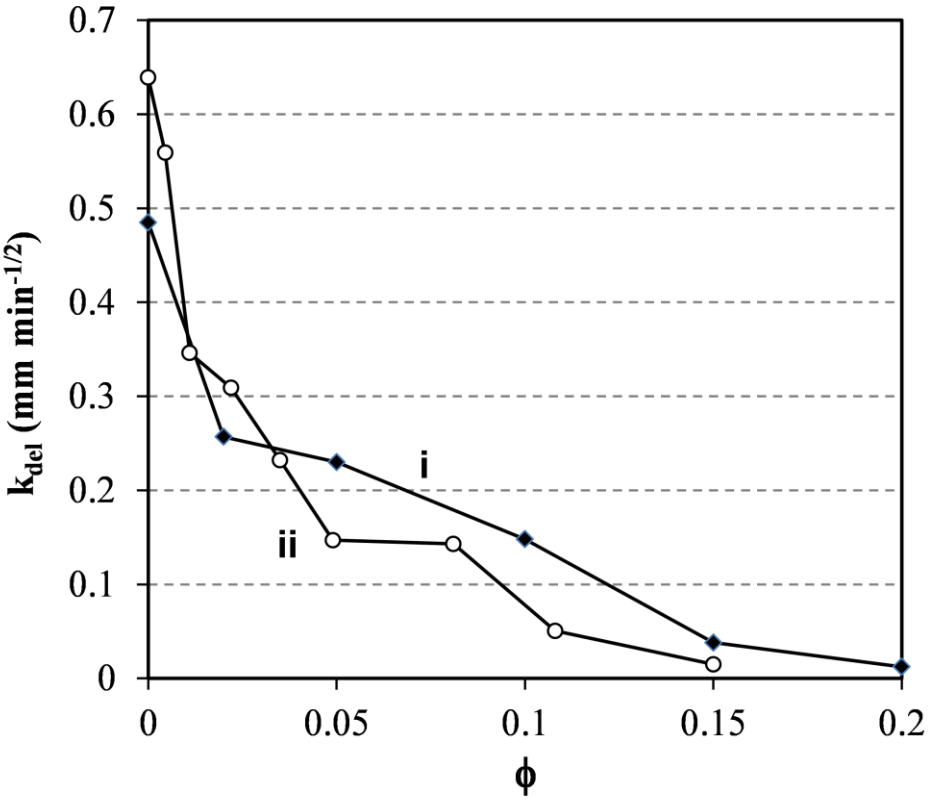

Figure 8

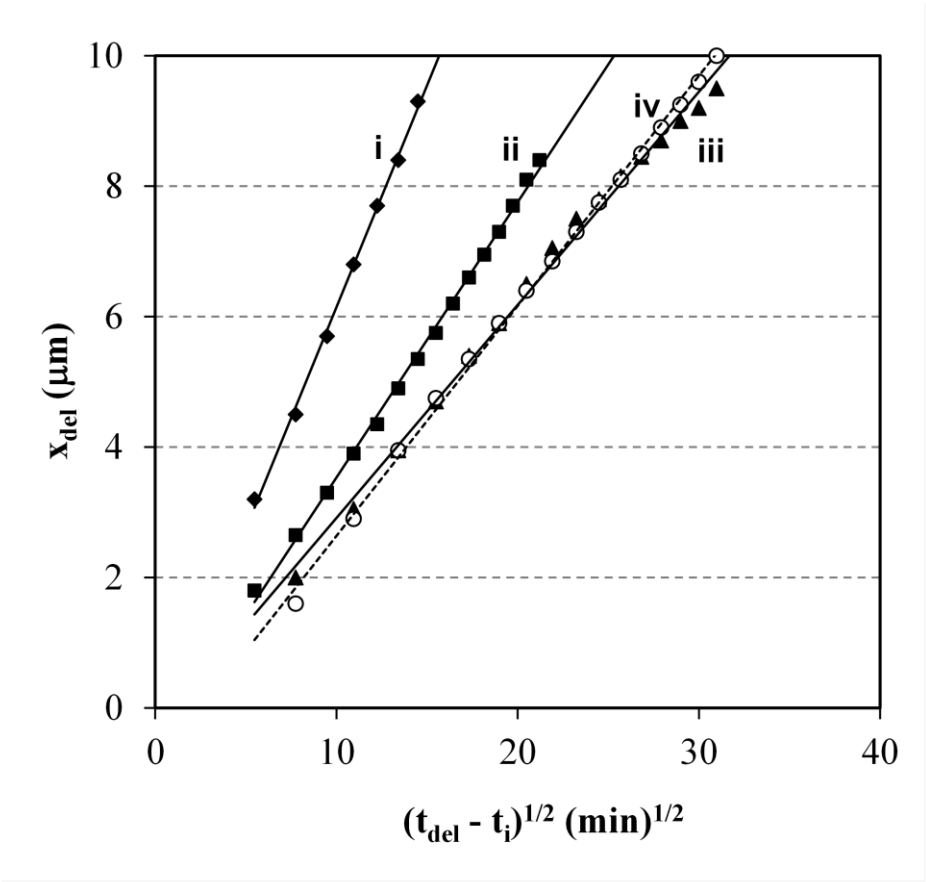

Figure 9

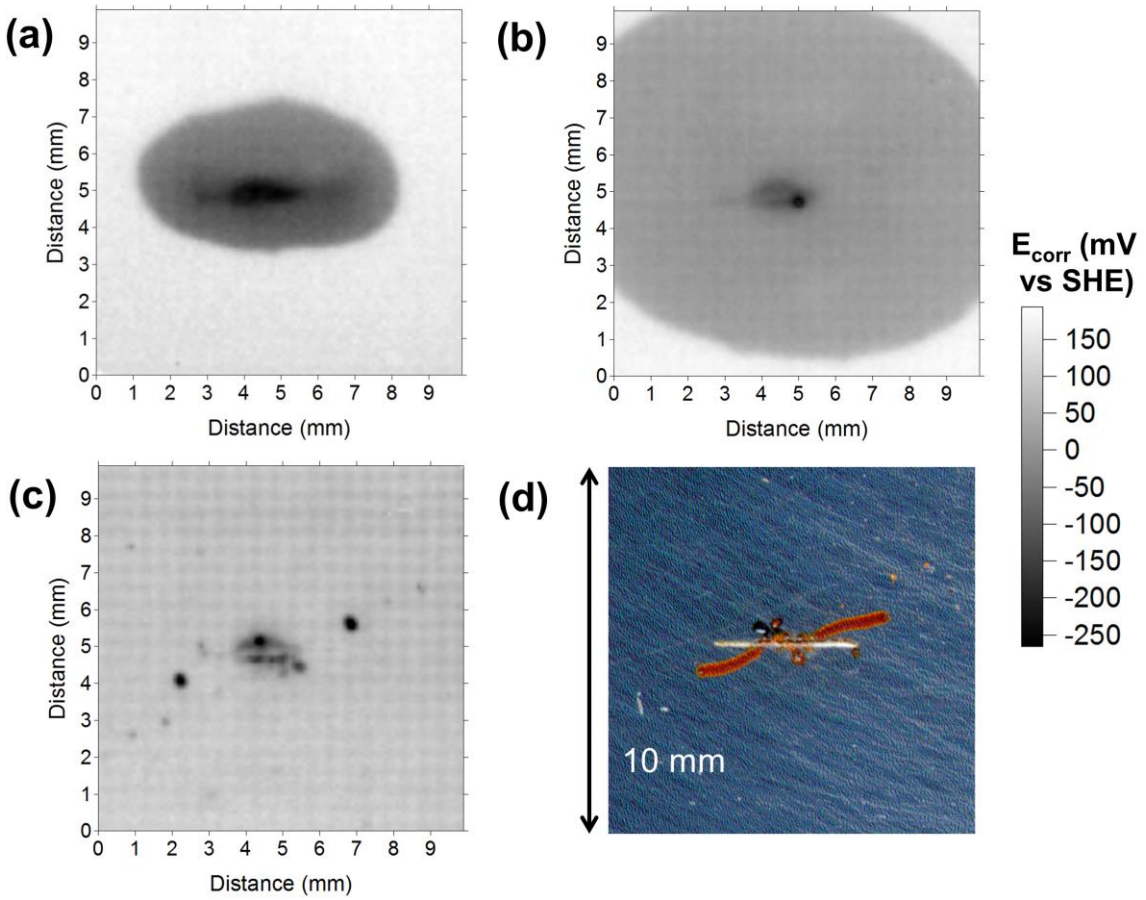
(a)
(b)
(c)
(d)
Distance (mm)
Distance (mm)
Distance (mm)
Distance (mm)
E_{corr} (mV vs SHE)
150
100
50
0
-50
-100
-150
-200
-250
10 mm

Figure 10

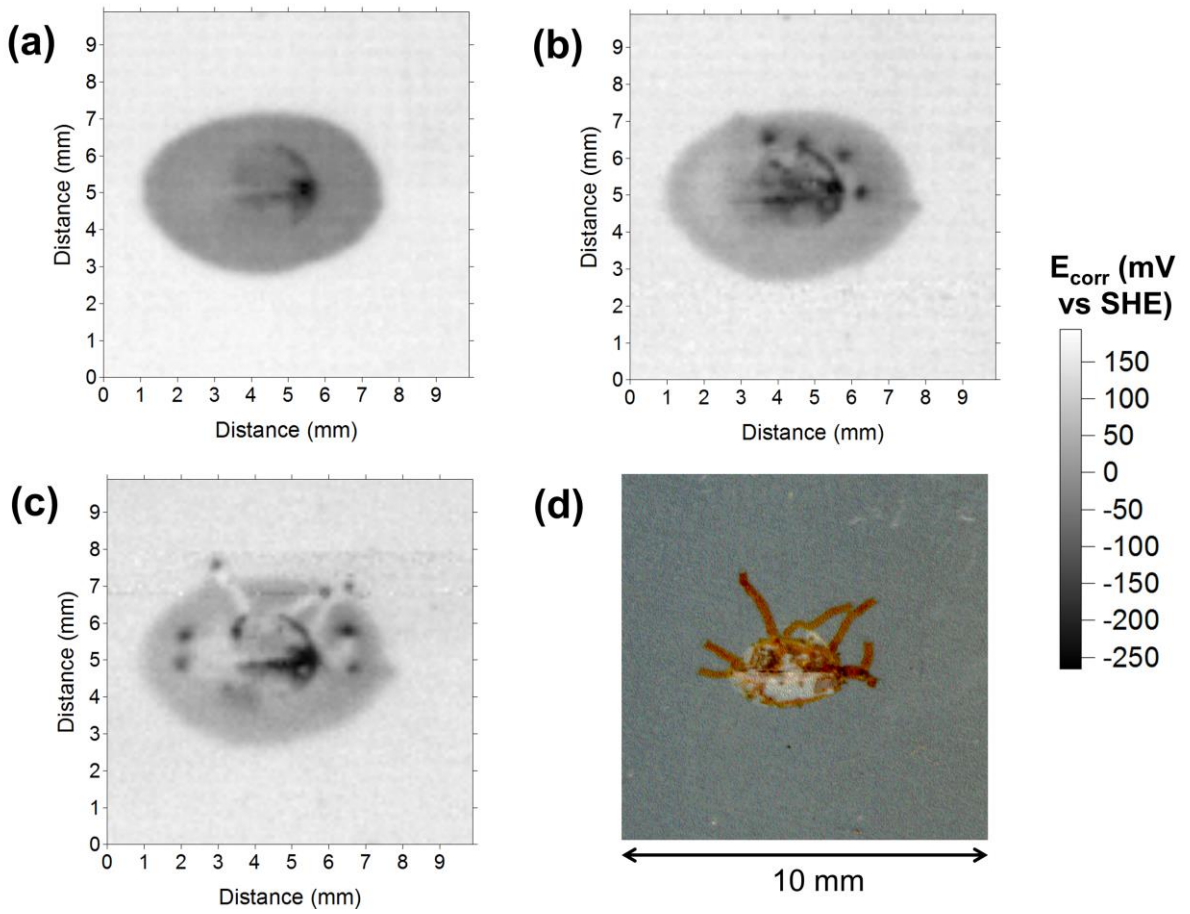
(a)
(b)
(c)
(d)
Distance (mm)
0 1 2 3 4 5 6 7 8 9
E_{corr} (mV vs SHE)
150
100
50
0
-50
-100
-150
-200
-250
10 mm

Figure 11

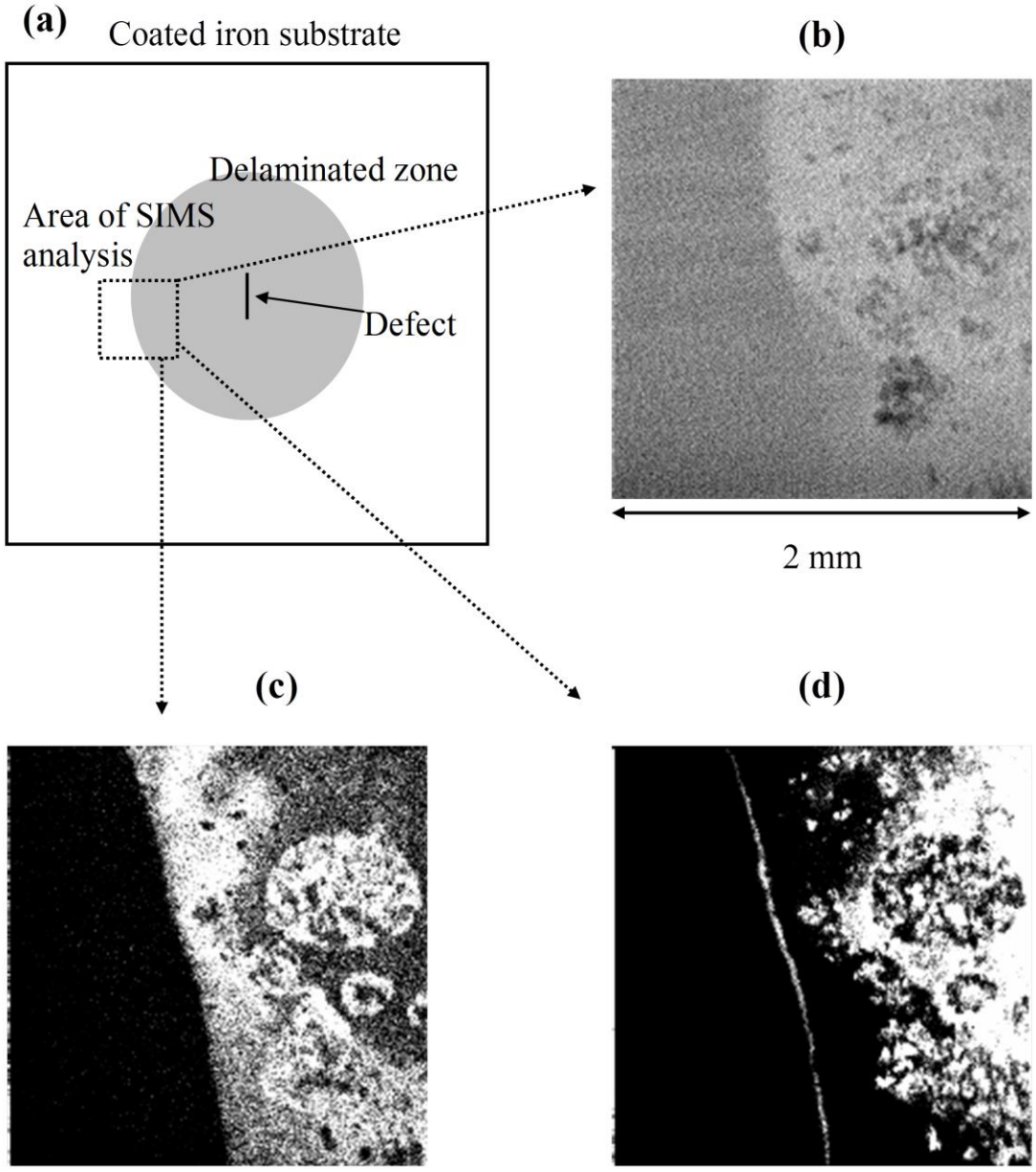
(a)
Coated iron substrate
Delaminated zone
Area of SIMS analysis
Defect
(b)
2 mm
(c)
(d)

Figure 12

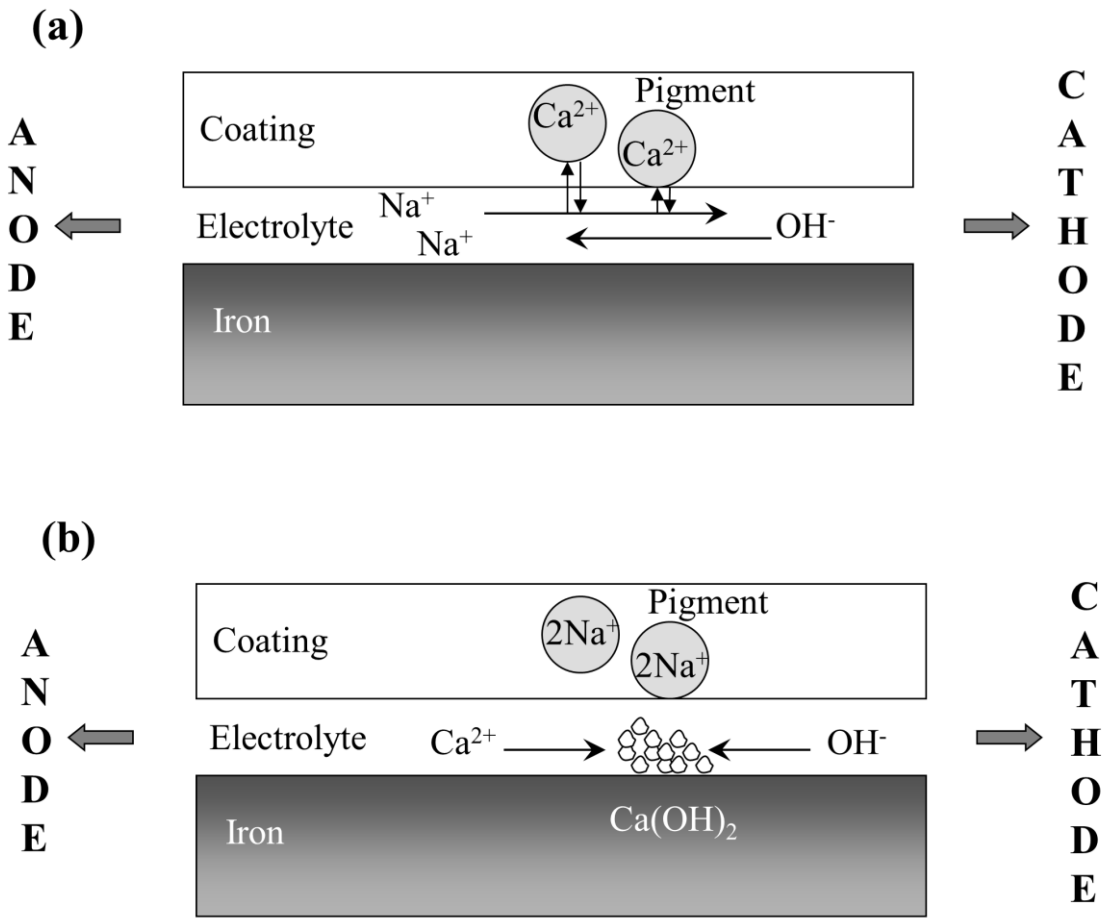
(a)
ANODE
Coating
Pigment
Ca2+
Ca2+
Electrolyte
Na+
Na+
OH-
Iron
CATHODE
(b)
ANODE
Coating
Pigment
2Na+
2Na+
Electrolyte
Ca2+
OH-
Iron
Ca(OH)2
CATHODE

Figure 13

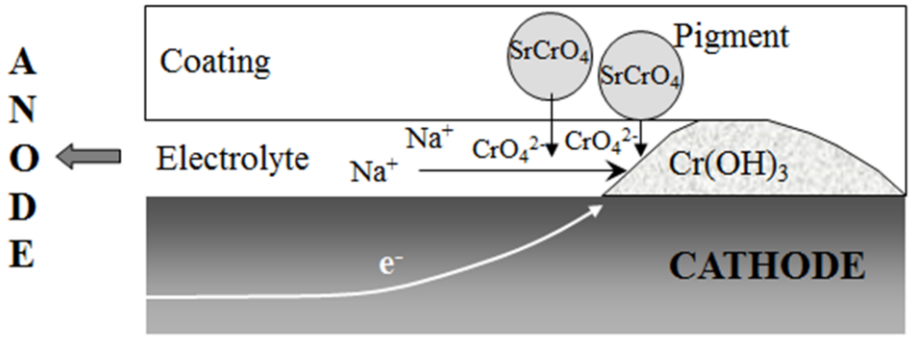
ANODE
Coating
SrCrO4
SrCrO4
Pigment
Electrolyte
Na+
Na+
CrO4 2-
CrO4 2-
Cr(OH)3
e-
CATHODE